engineering proceedings

MDPI

Proceeding Paper

Design and Optimization of an Aerospace Metamaterial Sandwich Panel †

Pierluigi Fanelli [1,*], Emanuele Vincenzo Arcieri [2], Andrea Ciula [1], Cristiano Biagioli [3], Barbara Mandolesi [3], Valerio Gioachino Belardi [3], Chiara Stefanini [1], Sergio Baragetti [2] and Francesco Vivio [3]

[1] Department of Economy, Engineering, Society and Business Organization (DEIm), University of Tuscia (UNITUS), Largo dell'Università, 01100 Viterbo, Italy; andrea.ciula@unitus.it (A.C.); chiara.stefanini@unitus.it (C.S.)
[2] Department of Management, Information and Production Engineering, University of Bergamo, Viale Marconi 5, 24044 Dalmine, Italy; emanuelevincenzo.arcieri@unibg.it (E.V.A.); sergio.baragetti@unibg.it (S.B.)
[3] Department of Enterprise Engineering, University of Rome Tor Vergata, Via del Politecnico 1, 00133 Rome, Italy; cristiano.biagioli@uniroma2.it (C.B.); barbara.mandolesi@uniroma2.it (B.M.); valerio.belardi@uniroma2.it (V.G.B.); vivio@uniroma2.it (F.V.)
* Correspondence: pierluigi.fanelli@unitus.it
† Presented at the 54th Conference of the Italian Scientific Society of Mechanical Engineering Design (AIAS 2025), Florence, Italy, 3–6 September 2025.

Abstract

This study investigates the structural behavior of metamaterial sandwich panels with Bézier-based lattice cores using parametric finite element modeling. Geometric parameters were varied to assess their influence on mass, stress, and energy absorption capabilities. Ligament thickness was found to strongly affect mass, while curvature influences stress and deformability. The optimization results outline a set of optimal design solutions, enabling selection of configurations based on specific performance priorities. The proposed workflow provides a robust strategy for designing mechanically efficient structures suitable for advanced engineering applications.

Keywords: metamaterials; sandwich panels; optimization; structural behavior; FEM

1. Introduction

Mechanical metamaterials [1,2] are a class of rationally designed structures whose effective properties are governed by their internal architecture rather than their constituent materials. This design-led paradigm allows for the creation of structures with precisely tailored and often unusual multiphysics behaviors. By systematically modifying the geometric parameters of the repeating unit cell, it is possible to tune a wide range of effective properties, including stiffness, bulk modulus, functionally graded characteristics, and even extreme thermal expansion. This design freedom also extends to achieving unconventional responses such as negative stiffness, auxeticity (a negative Poisson's ratio), and complex couplings between deformations, such as compression and twist. The rapid advancement of additive manufacturing (AM) technologies has been a critical catalyst, providing the unprecedented design freedom necessary to realize these complex internal geometries and bring metamaterials from conceptual design to functional engineering applications [3,4]. Moreover, the response of these architected materials can be made programmable, enabling properties to be actively tuned or switched via external stimuli, such as temperature, or through mechanically induced instabilities like buckling.

Academic Editors: Nicola Bonora, Umberto Galietti, Luigi Bruno, Davide Castagnetti, Cristiana Del Prete, Mario Guagliano and Vigilio Fontanari

Published: 25 March 2026

Within the vast design space of metamaterials, the use of curved elements instead of traditional straight struts has proven to be a particularly fruitful avenue of research. Topologies incorporating curved beams can offer distinct advantages, including greater compliance, reduced stress concentrations at junctions, and improved energy absorption capabilities. Various parametric curves, such as circular arcs, sinusoids, NURBS, and B-splines, have been employed to synthesize novel architected materials. Among these, Bézier curves offer a compelling balance of design flexibility and simplicity, as their complex shapes are governed by a small number of control points. This parametric nature makes them exceptionally well-suited for tuning mechanical properties through the precise manipulation of a few geometric variables, thereby widening the achievable design space [5–7].

The forward problem—predicting the properties of a given geometry—is often addressed using analytical models based on beam theory, strain energy methods like Castigliano's second theorem, or computational approaches such as finite element (FE) analysis and homogenization. However, the more critical challenge from an application standpoint is the inverse problem: identifying an architecture that yields a specific, targeted response. This problem is often ill-posed, as multiple distinct geometries can result in identical mechanical properties. To this end, structural optimization techniques, including topology and shape optimization, have become indispensable tools. Isogeometric analysis (IGA), in particular, has emerged as a powerful framework that integrates computer-aided design (CAD) and analysis, enabling more accurate and efficient shape optimization by using the same NURBS basis functions that define the geometry [8–10].

This paper presents a framework for the design and systematic optimization of metamaterials based on unit cells constructed from cubic Bézier curves. By methodically tuning the geometric parameters that define the Bézier curve—namely, the control point positions—we establish clear structure–property relationships that govern the material's mechanical and physical response. Leveraging a combination of computational homogenization and parametric optimization, our work addresses the inverse design challenge for this class of materials. The ultimate goal is to create a robust design methodology that enables the generation of Bézier-based metamaterials with customized, on-demand multiphysics properties, thereby expanding their potential for advanced engineering applications.

2. Materials and Methods

This study is an extension of the work [6] and investigates a broader set of geometric configurations by combining two complementary stages. In the first stage, an extensive parametric exploration was performed through automated FE analyses in the ANSYS 2020 R2 Mechanical APDL solver in batch mode. In the second stage, a targeted multi-factor optimization was conducted with modeFRONTIER 2024R2 software combined with FE modeling in Abaqus 2022. The aim was to establish a hierarchy among input parameters and provide designers with a robust tool for multi-objective optimization.

The investigated structure is a sample of a sandwich panel that occupies a volume of 21 mm × 25 mm × 21 mm, with top and bottom skins having a thickness of 2 mm. The core is formed by four in-plane repetitions of an elementary unit cell along two orthogonal directions, where the unit cell consists of two anti-symmetric cubic Bézier curves rotated by 90°. The parameter λ, which is the distance between the endpoints of the base curve, is therefore equal to 21 mm/4 = 5.25 mm. The thickness of the 2D ligament, defined by the Bézier curve, was kept constant in the studied cell. The resulting geometry is extruded along the out-of-plane direction.

Assuming a reference system with its origin in $\mathbf{P}_0$ and the x-axis oriented as the segment $\mathbf{P}_0\mathbf{P}_3$, the control points are positioned as follows: $\mathbf{P}_0(0,0)$, $\mathbf{P}_3$ (λ, 0), $\mathbf{P}_1(x_1, y_1)$

https://doi.org/10.3390/engproc2026131010

and $\mathbf{P}_2(\lambda - x_1, -y_1)$, since the curve considered in this study is anti-symmetric. For the herein study, the chosen variables are the position of the control point $\mathbf{P}_1$ with respect to $\mathbf{P}_0$, defined by the coordinates x_1 and y_1, and the thickness s. The variables x_1 and y_1 were varied from 0.5 to 2.7 mm in 0.2 mm increments and s from 0.5 to 1.1 mm with increments of 0.1 mm, whose full combination results in a total of 864 design configurations. In the optimization stage, each input variable was varied with the finer resolution of 0.1 mm while maintaining the same bounds. The range for s was determined based on the constraint $s/\lambda < 0.3$, which preserves topological integrity as indicated in [6].

Cubic Bézier curves are defined by four control points, $\mathbf{P}_0$, $\mathbf{P}_1$, $\mathbf{P}_2$ and $\mathbf{P}_3$ (Figure 1), according to Equation (1):

$$\mathbf{C}(u) = (1-u)^3\mathbf{P}_0 + 3u(1-u)^2\mathbf{P}_1 + 3u^2(1-u)\mathbf{P}_2 + u^3\mathbf{P}_3,\ u \in [0,1]. \quad (1)$$

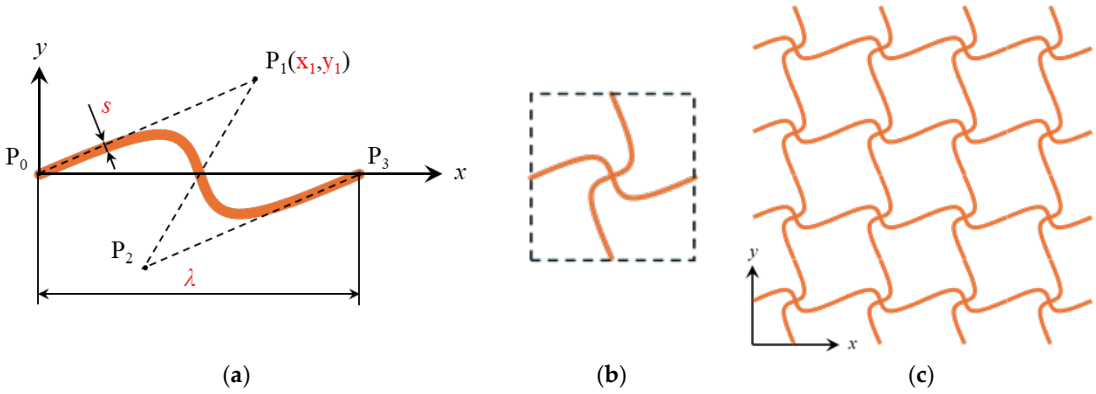

Figure 1. (**a**) Anti-symmetric cubic Bézier curve; (**b**) elementary cell; (**c**) metamaterial pattern.

The FE model was developed in APDL and Abaqus using 2D plane strain elements. In APDL, a fully structured quadrilateral mesh was employed, with the element size defined parametrically as one quarter of the cell thickness, varying with each configuration. In Abaqus, a uniform global mesh size of 0.05 mm was adopted for all models. The geometry of the Bézier curve was defined parametrically, allowing dynamic shape control via the definition of the coordinates of $\mathbf{P}_1$. The base curve (Figure 1a) was replicated by a 90° rotation to form the elementary cell (Figure 1b). The elementary cell was then repeated along the x- and y-directions to construct the whole sample (Figure 1c).

The sample was considered made of PLA. A homogeneous, isotropic, linear elastic material was considered, with E = 3500 MPa, ν = 0.36, and density ρ = 1230 kg/m^3. A general static analysis was performed with geometric nonlinearity taken into account. The lower surface of the bottom skin was fixed, and a uniform pressure of 0.1 MPa was applied on the top skin (Figure 2). No symmetry or periodic boundary conditions were applied at the sides, since the FE models represent samples of the sandwich structure rather than the entire sandwich panel.

To assess the structural behavior of the lattice structure, the following outputs were considered: maximum von Mises stress, maximum displacements in the x- and y-directions shown in Figure 2 (U1 and U2, respectively), strain energy and mass. Insights gained from the exploration analyses later inspired the definition of a variant design, discussed in Section 3.

Optimization was conducted using modeFRONTIER software, which interfaced with Abaqus through the workflow shown in Figure 3. The three input parameters (x_1, y_1 and s) were linked to the FE model, enabling automated generation and evaluation of design variants. Three optimization objectives were defined: (i) maximizing energy absorption, (ii) minimizing mass, and (iii) minimizing von Mises stress. The aim of the research

is to provide designers with design strategies tailored to the desired performance, i.e., a highly deformable, lightweight, or resistant structure. These three objectives could be conflicting, and for this reason a trade-off among the optimal geometries should be identified. The multi-strategy algorithm pilOPT was selected, and 100 combinations of the input parameters were tested.

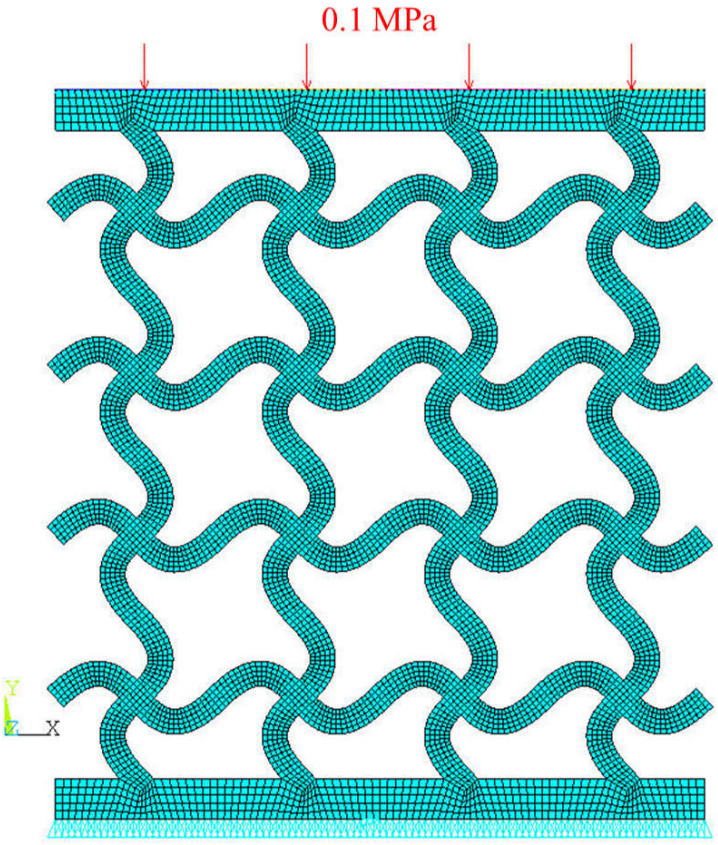

Figure 2. Loading and boundary conditions: pressure at the top skin and constraint at the bottom skin.

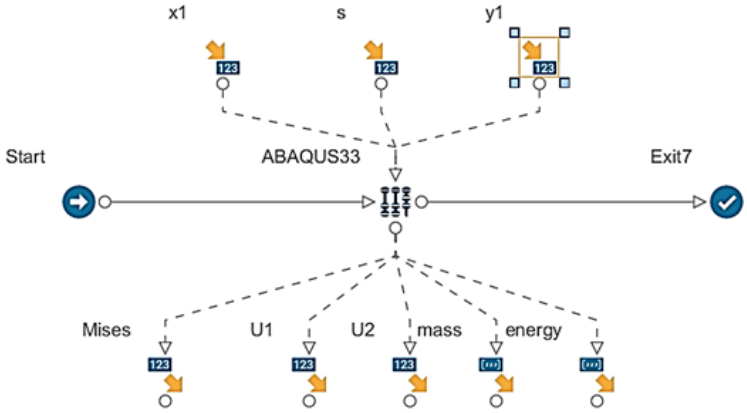

Figure 3. Workflow in modeFRONTIER. The process starts at the Start node and ends at Exit7. Input variables are shown at the top of the diagram, and the output variables at the bottom. The analyses are executed in Abaqus (central node). The finite element models are generated from the input variables and the output variables are extracted at the end of each simulation.

3. Results and Discussion

To explore correlations among input and output parameters, scatter matrix analysis was employed. A scatter matrix (Figure 4) is a square matrix whose size corresponds to the number of parameters considered. The input (s, x_1, y_1) and output (strain energy,

mass, maximum von Mises stress, U1, U2) parameters are ordered and assigned to the rows and columns. The diagonal elements contain histograms showing the distribution of each parameter across all simulations, while the panels above the diagonal display the corresponding pairwise scatter plots for the parameters in the associated row and column. Below the matrix diagonal, the relationships between each pair of parameters are summarized through the Pearson correlation coefficient, with color intensity indicating the strength and sign of each correlation. Values of correlation coefficients near +1 (red) indicate a strong direct relationship between variables, while values near −1 (blue) reflect a strong inverse relationship. Coefficients close to 0 (white) suggest a negligible correlation between the variable pair. By showing, for each parameter pair, both the scatter plot and its corresponding correlation coefficient, the scatter matrix makes it straightforward to judge whether the relationship is truly linear and how closely the data align with a linear trend, something that either plot or correlation alone does not convey as clearly.

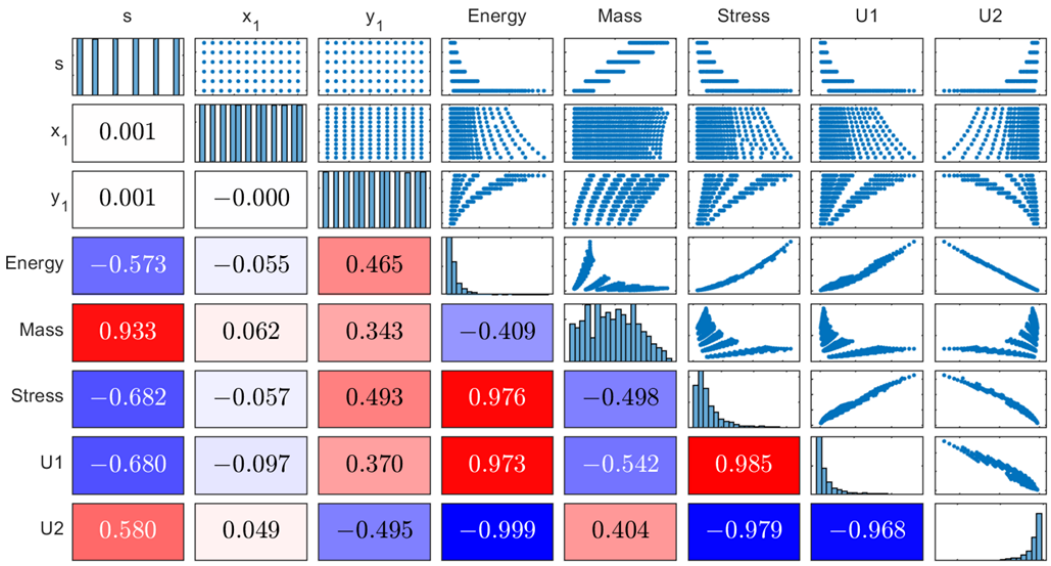

Figure 4. Scatter matrix—APDL parametric exploration.

Among the three geometric input parameters, the ligament thickness, s, exhibits the strongest overall influence. Its highest positive correlation is with the total mass (correlation factor = +0.933), highlighting that configurations with thicker ligaments are inherently heavier. Other notable correlations of s with output parameters are negative, indicating that thicker morphologies tend to experience lower peak stress (−0.682) and reduced deformation (0.580 vertical and −0.680 horizontal) and therefore store less strain energy (−0.573). Following s, the most influential parameter is y_1, whose correlations with the output variables are moderate (between 0.3 and 0.5 in module). Increasing y_1, corresponding to more curved ligaments, generally leads to more deformable and energy-absorbing configurations but with higher stresses and mass, though the trends are less pronounced than those associated with s. The negative correlation for U2 reflects the convention adopted in the model, where positive U2 is defined in the upward direction. The parameter x_1 shows negligible effects, with all correlation coefficients within −0.1 and +0.1.

Beyond these quantitative trends, the scatter plots reveal that combinations of small s or large y_1 do not yield univocal performance patterns—except for the clear linear relationship between s and mass—suggesting multiple feasible solutions in those regions of the design space. Moreover, strong interdependencies are evident among the output quantities themselves: lateral and vertical displacements are strongly correlated, strain

energy increases with both displacements and stresses, and stresses and displacements are likewise mutually correlated.

A bubble chart (Figure 5) was used to simultaneously visualize three output variables, i.e., mass, strain energy, and maximum von Mises stress, to visualize their mutual correlations and how they are affected by the input parameters. Each set of input parameters is represented in the energy–mass plane, with size and color both indicating the level of von Mises stress. The analysis shows the presence of a Pareto front, indicating trade-offs among the performance metrics. The influence of the three input parameters (x_1, y_1, and s) is annotated on the chart with arrows, highlighting how increments in each parameter shift the overall trend in the performance space.

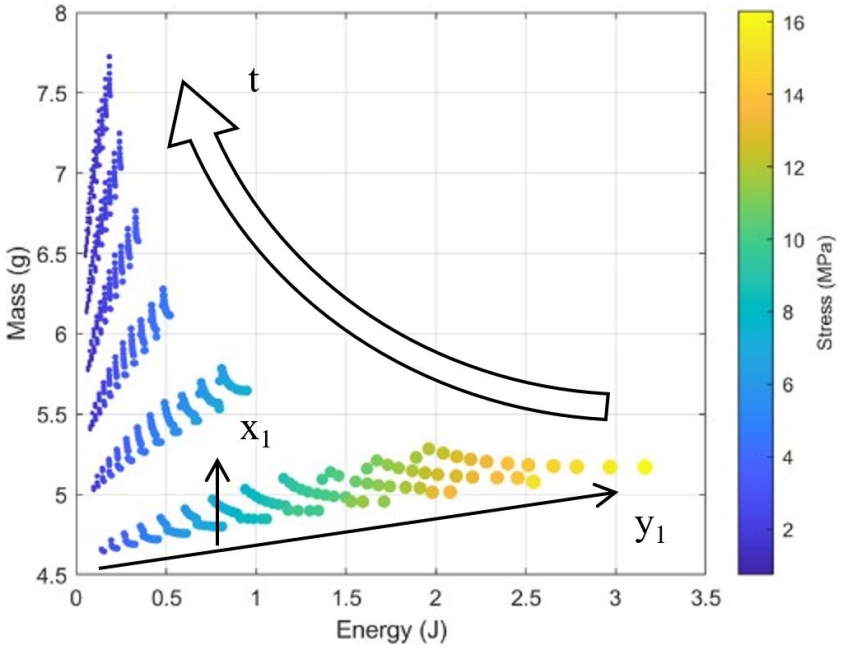

Figure 5. Bubble chart—APDL, with annotated influences of input parameters.

As already observed from the scatter matrix analysis, the strain energy and von Mises stress are strongly correlated (0.976), confirming that configurations experiencing higher stresses also store greater strain energy. The hierarchy among the geometric parameters influencing performance is consistent with previous findings: the ligament thickness s governs the overall mechanical behavior and modulates the extent to which y_1 can affect the structural response, whereas x_1 shows only a marginal influence. Varying y_1 at low s values allows modulation of energy and stress at low mass, whereas changing y_1 at high s values mainly affects the mass while keeping stresses and strain energy relatively low.

Following the observations from the parametric analysis, a balanced variant of the morphology was developed by slightly modifying the geometry to suppress the lateral displacement U1 detected in the original configuration, which is due to the anti-symmetric nature of the base curve geometry. Assuming that such an effect was mainly caused by the ligaments extending along the vertical (load) direction, the design objective was to achieve an alternation of mirrored vertical ligaments. Since the mirroring of the vertical ligaments alone results in geometrical incompatibilities at the modified cell centers (Figure 6), this configuration was obtained by alternating the mirroring of the entire unit cells (Figure 7). The corner joint at the junction between the horizontal ligaments of adjacent cells (Figure 7a), introduced by mirroring the entire cells, represents a geometric discontinuity, which was resolved by reshaping the horizontal Bézier curves. The end control points $\mathbf{P}_0$ and $\mathbf{P}_3$ were repositioned to align horizontally with the inner control points $\mathbf{P}_1$ and $\mathbf{P}_2$, respectively

https://doi.org/10.3390/engproc2026131010

(Figure 7b). This adjustment ensured horizontal tangency at the cell boundaries, restoring geometric continuity between neighboring ligaments. Subsequently, a consistent shift of all control points vertically towards the origin was performed, with the vertical coordinate being reduced by half. This resulted in a more regular, almost orthogonal intersection with the vertical lines, resulting in a symmetric arrangement (Figure 7c) that compensates for the lateral offset observed in the original pattern.

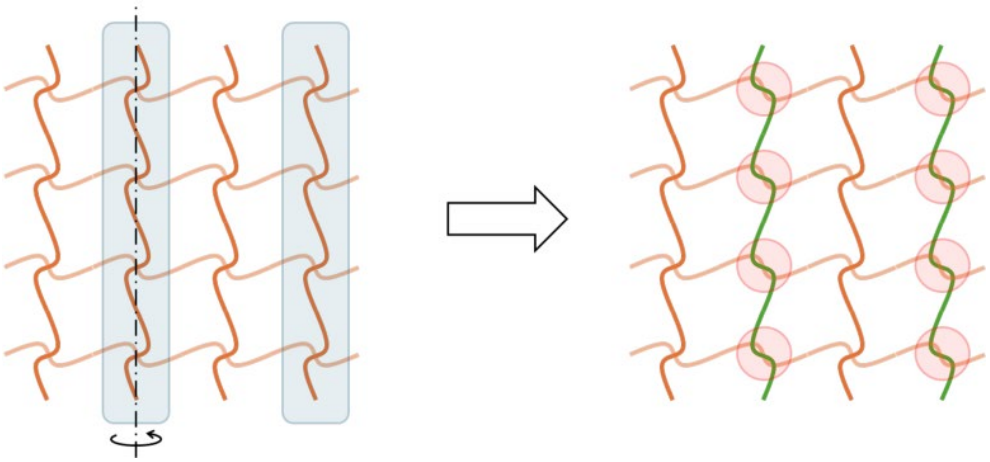

Figure 6. Alternating the mirroring of the vertical ligaments alone (green) results in geometrical incompatibility at the intersections; thus, the entire cells need to be mirrored.

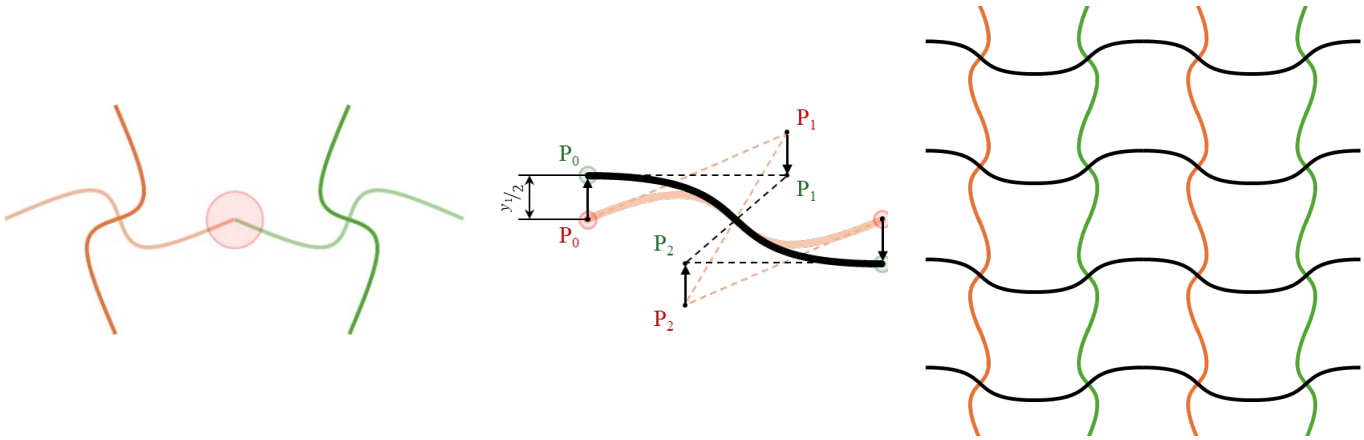

(**a**) (**b**) (**c**)

Figure 7. By mirroring the entire cell and slightly adjusting the control points of the horizontal Bézier curves, a balanced cell was defined without significantly altering the geometry of the original morphology: (**a**) angle joint between the horizontal ligaments of adjacent cells; (**b**) reshaping of the horizontal ligament by adjusting the control points; and (**c**) resulting balanced configuration pattern.

To assess the effect of the geometric modification, the same parametric campaign was repeated using the balanced morphology. The analysis followed exactly the same procedure, varying the same set of input parameters and evaluating the corresponding mechanical outputs under identical boundary conditions. The results are again represented through a scatter matrix analysis, enabling a direct comparison with the previous dataset and revealing how the geometric adjustments influence the correlations among performance metrics.

The results obtained with the balanced morphology (Figure 8) are largely consistent with those of the sample using the original cell (Figure 4) in terms of correlations and overall trends observed in the scatter plots. The relationships among the main geometric and performance variables remain essentially unchanged, confirming that the modification did

not alter the mechanical behavior of the structure. The only significant difference concerns the lateral displacement U1, which is effectively suppressed in the balanced configuration, demonstrating the success of the geometric correction.

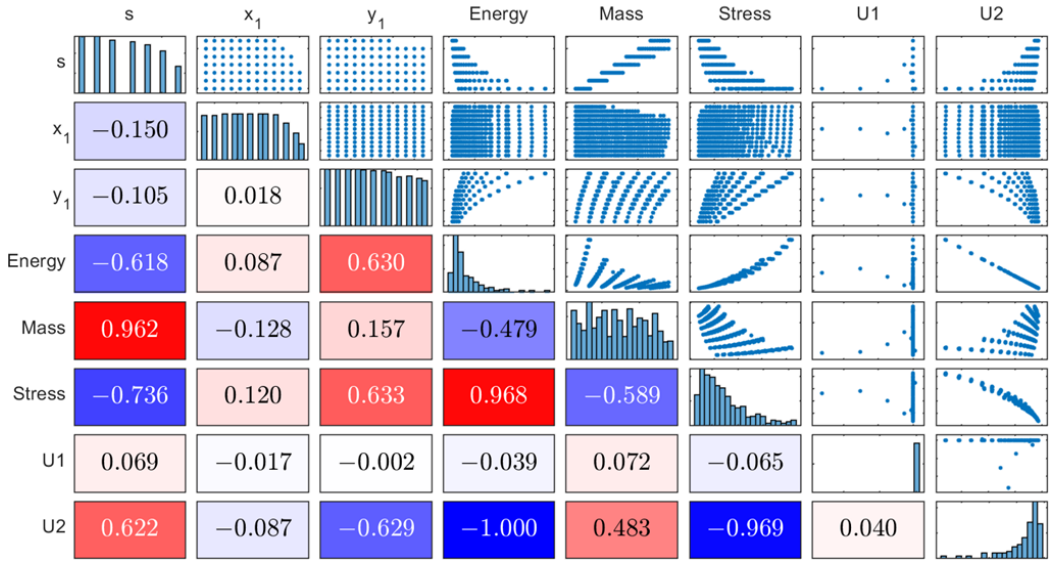

Figure 8. Scatter matrix—APDL parametric exploration with the newly introduced design. A small number of configurations are missing from the dataset, as the corresponding analyses were not successfully executed during the automated batch process and are therefore not included in the presented results.

The comparison of von Mises equivalent stress and deformation fields between the two morphologies shown in Figure 9 refers to a configuration with a specific set of input parameters: s = 0.5 mm, x_1 = 2.2 mm and y_1 = 2.2 mm. The balanced configuration effectively eliminates the lateral displacement observed in the unbalanced case, which reached approximately 5 mm. This improvement, however, comes at the cost of a generally higher stress level, as a larger portion of material now actively contributes to carrying the load, including regions that previously sustained limited stress, such as the vertical ligaments directly connected to the top and bottom plates. As a result, the peak von Mises stress increases by about 27% compared to the unbalanced configuration (14.4 MPa versus 11.3 MPa).

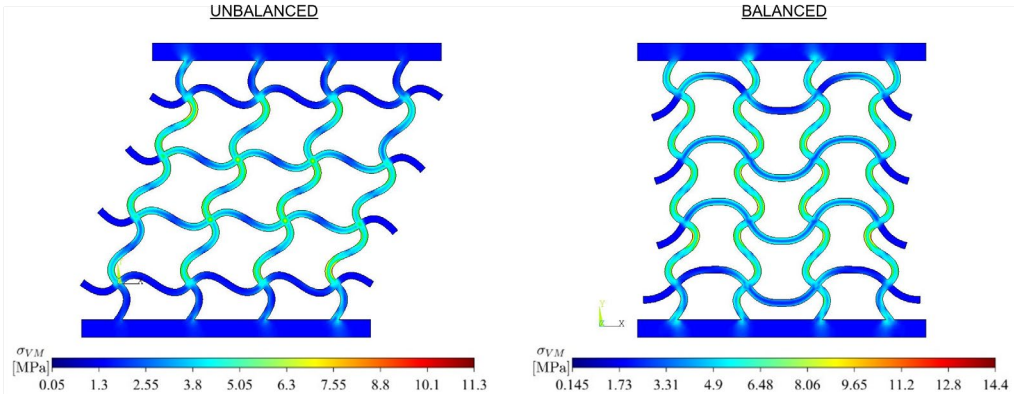

Figure 9. Comparison of von Mises stress distribution (averaged element solution) and overall displacements between original unbalanced morphology (left) and balanced cell (right) for a reference configuration having s = 0.5 mm, x_1 = 2.2 mm and y_1 = 2.2 mm. The balanced configuration exhibits a maximum displacement of 5.56 mm, in contrast with the smaller, purely vertical maximum displacement of 2.68 mm observed in the balanced configuration.

https://doi.org/10.3390/engproc2026131010

In addition, the rotation of the cantilevered ligaments on the sides of the balanced FE model can be clearly observed in Figure 10, indicating rotation at the central intersection of the side cells. This behavior, together with the tendency of the intersections to move closer toward the specimen center in the horizontal direction, provides clear evidence of the auxetic nature of the balanced morphology. Although this tendency is partially constrained by the two skins, it remains visible at mid-height along the lateral edges of the model.

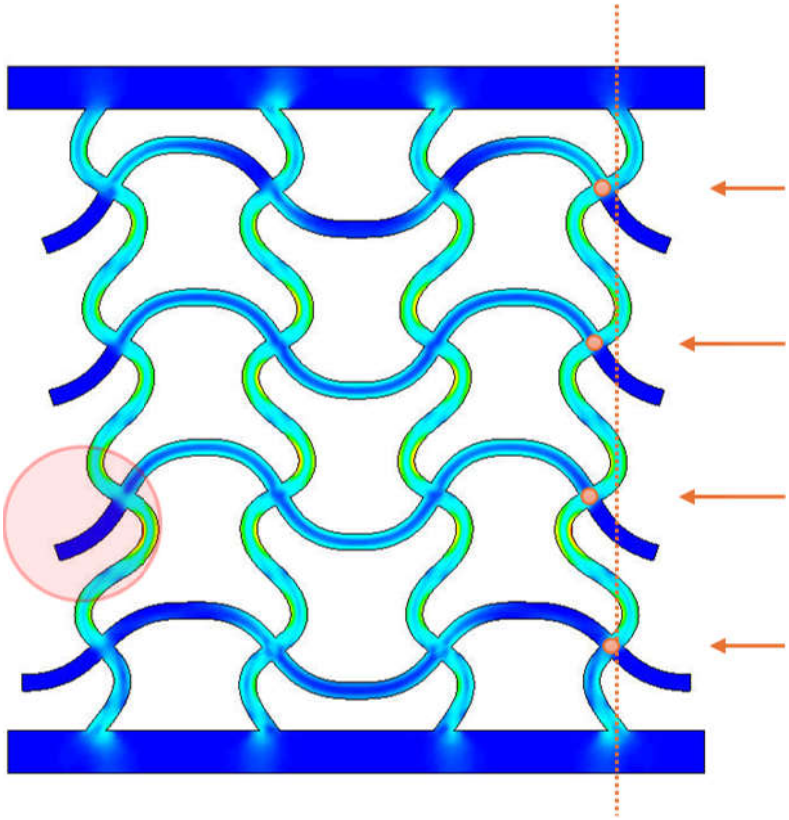

Figure 10. New balanced morphology showing auxeticity behavior (as shown by the shift of the cell centers on the right relative to the dotted vertical line, indicated by arrows) and rotation of the intersection at the center of the elementary cells, more readily apparent in the side cells, where the cantilevered ligaments are dragged by the cell's central junction following rotation with rigid motion (circled in red).

The optimization analysis was performed on the original (unbalanced) cell morphology to validate the connection between the FE model and the optimization environment. The scatter matrix obtained from the optimization stage (Figure 11) exhibits correlation factors and trends nearly identical to those observed in the exploratory parametric campaign, confirming the consistency of the two approaches. In particular, a strong positive correlation is found between mass and ligament thickness s (0.972), pointing out the dominant role of s in determining the material volume. The geometric parameters x_1 and y_1 show weaker correlations with mass, as the correlation values are 0.174 and 0.405, respectively. The parameter x_1 shows negligible correlation with all output variables, with coefficients between −0.2 and +0.2, suggesting minimal correlation with mechanical behavior. The parameter y_1 has a partial correlation with structural behavior, as it directly affects the curvature of the Bézier ligament and consequently the stress distribution and deformability. Higher values of y_1 are associated with higher von Mises stress (0.639), increased strain energy (0.561), and higher vertical displacement U2 (−0.542).

https://doi.org/10.3390/engproc2026131010

Figure 11. Scatter matrix—Abaqus–modeFRONTIER optimization analysis. The structure of this scatter matrix is the same as in Figures 4 and 8. Red markers are used in the histograms and scatter plots to indicate failed simulations.

Overall, the optimization model successfully reproduces the trends and correlations identified in the full-factorial study, while requiring approximately one order of magnitude fewer iterations. This demonstrates the reliability and computational efficiency of the coupled Abaqus–modeFRONTIER optimization analysis in capturing the same physical relationships with a substantially reduced number of simulations.

The analysis shows the presence of the previously identified Pareto front rather than a single optimal design since a multi-objective optimization was performed. Selection of geometrical parameters for the lattice structure depends on design priorities, i.e., resistance, deformability, or lightweight. The design defined by s = 0.5 mm and y_1 = 0.5 mm, at the same time, leads to low values of mass, absorbed energy, and stress. The combination of s = 0.5 mm and y_1 = 2.7 mm provides results where high energy absorption capabilities are obtained, with low mass but high stresses. A configuration with s = 1.1 mm and y_1 = 0.5 mm results in low stresses, low energy, and high mass.

4. Conclusions

This study investigated the structural behavior of metamaterial sandwich panels with cores based on anti-symmetric cubic Bézier curves. Through parametric FE modeling, a systematic framework was developed to assess the influence of geometric parameters and guide the selection of mechanically efficient configurations. The analysis revealed that ligament thickness is the dominant parameter influencing mass. The horizontal position of the inner control points has negligible impact on mechanical performance, suggesting limited relevance in structural optimization within the tested range. In contrast, the vertical position significantly affects stress distribution and deformability, with higher values associated with increased von Mises stress and strain energy. Multi-objective optimization yielded a Pareto front of best designs, enabling tailored trade-offs between mass, stress, and energy absorption. Depending on design priorities, i.e., lightweight, stress minimization, or high energy absorption capabilities, optimal configurations can be achieved through targeted parameter selection. The proposed workflow offers a robust

approach to lattice structure optimization, which contributes to the development of high-performance components for advanced engineering applications. In addition, a balanced morphological variant was introduced to eliminate the lateral displacement observed in the original configuration. The geometric modification, based on alternating mirrored cells and adjusted Bézier boundaries, effectively suppressed the undesired motion while preserving the overall mechanical behavior. Although slightly higher stress levels were observed, the balanced configuration ensured a symmetric deformation pattern and improved global stability under compression.

Author Contributions: Conceptualization, P.F., A.C., E.V.A., and C.B.; methodology, P.F., A.C., E.V.A., and F.V.; software, A.C. and B.M.; validation, E.V.A. and S.B.; formal analysis, A.C. and E.V.A.; investigation, P.F., A.C., E.V.A., and S.B.; resources, P.F., A.C., and E.V.A.; data curation, A.C. and E.V.A.; writing—original draft preparation, V.G.B., A.C., and E.V.A.; writing—review and editing, C.S., P.F., and A.C.; visualization, V.G.B., A.C., and E.V.A.; supervision, P.F., F.V., and S.B.; project administration, P.F.; funding acquisition, P.F., E.V.A., and F.V. All authors have read and agreed to the published version of the manuscript.

Funding: The activity was conducted within the project "Innovative multiphysical approach to aerospace metamaterials design"—PRIN 2022 PNRR (DD MUR n.1409 del 14-9-2022), funded by the European Union—NextGenerationEU—M4, C2, 1.1.—CUP: J53D23015840001.

Institutional Review Board Statement: Not applicable.

Informed Consent Statement: Not applicable.

Data Availability Statement: Data are available upon request.

Conflicts of Interest: The authors declare no conflicts of interest.

References

1. Barchiesi, E.; Spagnuolo, M.; Placidi, L. Mechanical Metamaterials: A State of the Art. *Math. Mech. Solids* **2019**, *24*, 212–234. [CrossRef]
2. Surjadi, J.U.; Gao, L.; Du, H.; Li, X.; Xiong, X.; Fang, N.X.; Lu, Y. Mechanical Metamaterials and Their Engineering Applications. *Adv. Eng. Mater.* **2019**, *21*, 1800864. [CrossRef]
3. Askari, M.; Hutchins, D.A.; Thomas, P.J.; Astolfi, L.; Watson, R.L.; Abdi, M.; Ricci, M.; Laureti, S.; Nie, L.; Freear, S.; et al. Additive Manufacturing of Metamaterials: A Review. *Addit. Manuf.* **2020**, *36*, 101562. [CrossRef]
4. Saunders, R. *Metamaterials Using Additive Manufacturing Technologies*; Naval Research Laboratory: Washington, DC, USA, 2020.
5. Felsch, G.; Ghavidelnia, N.; Schwarz, D.; Slesarenko, V. Controlling Auxeticity in Curved-Beam Metamaterials via a Deep Generative Model. *Comput. Methods Appl. Mech. Eng.* **2023**, *410*, 116032. [CrossRef]
6. Álvarez-Trejo, A.; Cuan-Urquizo, E.; Roman-Flores, A. Effective Young's Modulus of Bézier-Based Honeycombs: Semi-Analytical Modeling and the Role of Design Parameters and Curvature. *Thin-Walled Struct.* **2023**, *192*, 111136. [CrossRef]
7. Álvarez-Trejo, A.; Cuan-Urquizo, E.; Roman-Flores, A.; Trapaga-Martinez, L.G.; Alvarado-Orozco, J.M. Bézier-Based Metamaterials: Synthesis, Mechanics and Additive Manufacturing. *Mater. Des.* **2021**, *199*, 109412. [CrossRef]
8. Wang, Z.-P.; Poh, L.H. Optimal Form and Size Characterization of Planar Isotropic Petal-Shaped Auxetics with Tunable Effective Properties Using IGA. *Compos. Struct.* **2018**, *201*, 486–502. [CrossRef]
9. Cho, S.; Ha, S.-H. Isogeometric Shape Design Optimization: Exact Geometry and Enhanced Sensitivity. *Struct. Multidiscip. Optim.* **2009**, *38*, 53–70. [CrossRef]
10. Choi, M.-J.; Cho, S. Isogeometric Configuration Design Optimization of Shape Memory Polymer Curved Beam Structures for Extremal Negative Poisson's Ratio. *Struct. Multidiscip. Optim.* **2018**, *58*, 1861–1883. [CrossRef]